ACS APPLIED MATERIALS & INTERFACES

Research Article

www.acsami.org

Facile Fabrication of a Three-Dimensional Cross-Linking TiO_2 Nanowire Network and Its Long-Term Cycling Life for Lithium Storage

Qin Hao,[†] Liang Chen,[‡] and Caixia Xu*[,†]

[†]Key Laboratory of Chemical Sensing and Analysis in Universities of Shandong, School of Chemistry and Chemical Engineering, University of Jinan, Jinan 250022, China

[‡]School of Chemistry and Chemical Engineering, Shandong University, Jinan 250100, China

Supporting Information

ABSTRACT: We describe a simple preparation of amorphous TiO_2 nanomaterial through a simple dealloying method with high throughput at room temperature. The as-made TiO_2 sample has a unique three-dimensional network structure built by cross-linking nanowires with the diameter of ~5 nm. As an anode material for Li-ion batteries, the TiO_2 product exhibits high capacities and a long cycling life at high rates of 500 and 1000 mA g^{-1}. In addition, it has a good rate capability. The as-made TiO_2 nanowire network shows great application potential as an anode material with the advantages of unique performance and easy preparation.

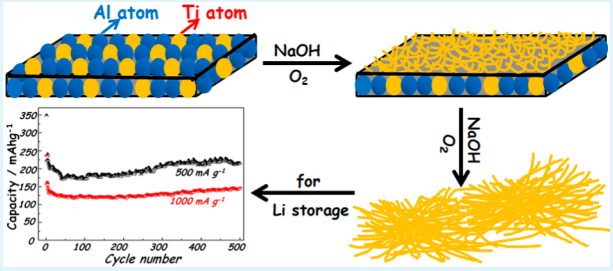

KEYWORDS: *titanium oxide, amorphous, dealloying, network structure, Li-ion batteries, anode material*

INTRODUCTION

Rechargeable lithium-ion batteries (LIBs) have allowed the wireless revolution of phones, computers, and digital cameras, which have transformed global communication because of their excellent performance.[1,2] It is well-known that the performance of LIBs is primarily determined by electrode materials. At present, the commercial anode material is graphite, but its low capacity (372 mA h g^{-1}) has restricted the application of LIBs in high-power fields.[3,4] Therefore, great effort has been spent to explore the substitutable anode candidates. Metal oxides have represented an interesting class of anode materials because of their high capacities.[5] Among various metal oxide materials, TiO_2 has been studied extensively because of its high stability, rich abundance, and nontoxicity. Various crystalline polymorphs, including anatase, rutile, TiO_2[B] (bronze), amorphous phase, etc.,[6−9] have been thoroughly investigated. Therein, amorphous TiO_2 was reported to perform excellently with a high capacity and long cycling life. However, amorphous TiO_2 has not become a focus of general research interest.

It is known to us that the size and morphology have significant effects on the performance of electrode materials. At present, many nanostructured TiO_2 materials, such as nanoparticles, nanotubes, nanowires, and porous structures, were designed to improve their electrochemical performance for LIBs.[6−11] Meanwhile, many preparation methods have also been proposed, such as sol−gel, chemical vapor deposition, anodic oxidation, and solvothermal methods.[6−16] These methods always involve high-temperature processing, an excessive use of capping or organic agents, etc. Therefore, it is desirable to use a simple and convinent method to fabricate TiO_2 under mild conditions, especially at room temperature. A corrosion route was developed by our group to prepare nanostructured metal oxides, such as Mn_3O_4 and Co_3O_4.[17,18] This method requires only the immersion of a binary alloy in a corrosive solution to selectively dissolve one element under ambient atmospheric conditions. It has proven to be an effective and simple method for fabricating metal oxides in high yield with no organic agents used.

In this work, we report the fabrication of a type of unique amorphous TiO_2 nanomaterial in high throughput via a simple dealloying method. The as-made sample has a three-dimensional network structure built by cross-linking TiO_2 nanowires, which exhibits a high capacity, a long cycle life, and good rate capability. Experimetal results demonstrate that the as-made TiO_2 sample shows promising application potential as an anode material for LIBs.

EXPERIMENTAL SECTION

Sample Preparation. High-purity Ti and Al (99.9%) metals were weighted in a 15:85 ratio, and then these metals were refined in an arc-furnace, followed by melt-spinning at 1600 r under a protective Ar atmosphere. Finally, $Ti_{15}Al_{85}$ (atom %) alloy foils with thicknesses of ~50 μm were prepared. In a typical dealloying experiment, a $Ti_{15}Al_{85}$ alloy foil was immersed in a 2 mol L^{-1} NaOH solution at room temperature for 72 h. Finally, the product was washed several times with ultrapure water (18.2 MΩ) and dried at room temperature in air.

Received: February 19, 2014
Accepted: June 9, 2014
Published: June 9, 2014

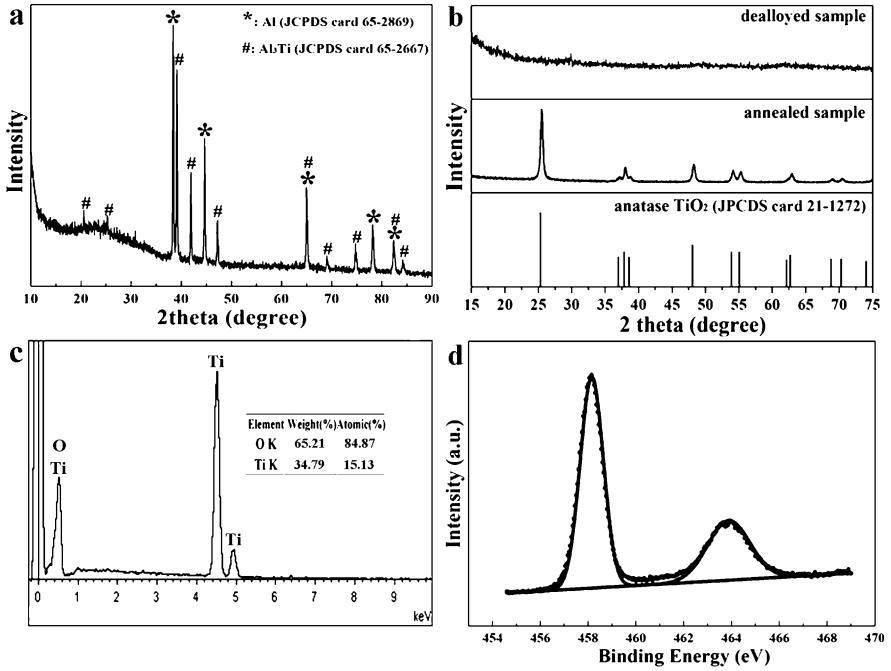

Figure 1. XRD patterns of (a) the TiAl alloy and (b) the dealloyed TiAl alloy in a 2 M NaOH solution for 72 h and the sample after it had been annealed and (c) EDS and (d) Ti 2p XPS spectra of the product obtained by etching for 72 h.

To prepare 1 g of TiO_2 sample, ~180 cm^2 of $Ti_{15}Al_{85}$ alloy foils was needed.

Characterization. Powder X-ray diffraction (XRD) was conducted with a Bruker D8 advanced X-ray diffractometer using Cu Ka radiation at a step rate of 0.04° s^{-1}. The morphology and structure of the product were observed through field emission scanning electron microscopy (SEM, JEOL JSM-7600F) with an energy-dispersive X-ray spectrometer (EDS) for compositional analysis. The elemental mapping was obtained using an FEI QUANTA FEG250 scanning electron microscope equipped with an INCA Energy X-MAX-50 X-ray spectroscopy analyzer. Transmission electron microscopy (TEM) images were obtained with a JEM-2100 high-resolution transmission electron microscope (200 kV). Surface structural properties of the amorphous TiO_2 were analyzed by means of an X-ray photoelectron spectrometer (ESCALab250), using a monochromatized MgKa X-ray as the excitation source and choosing C 1s (284.60 eV) as the reference line.

Electrochemical Tests. The electrochemical behavior versus Li was measured using coin-type cells (size of 2032). To prepare the working electrodes, the active TiO_2 powders, acetylene black, and carboxymethyl cellulose (CMC) were mixed in a 6:2:2 weight ratio in ultrapure water. After the slurry had been milled (QM-3SP2 Planetary Ball Mill) for 2 h, it was coated onto a piece of Cu foil and dried under vacuum at 80 °C for 12 h. The separator was a Celgard 2300 microporous membrane. The electrolyte was composed of 1 mol L^{-1} $LiPF_6$ dissolved in an ethylene carbonate (EC)/dimethyl carbonate (DMC)/ethylene methyl carbonate (EMC) mixture with a volume ratio of 1:1:1. The cells were constructed in an Ar-filled humidity-free glovebox. The cells were cycled galvanostatically between 0.01 and 3 V using a NEWARE BTS 5 V-50 mA computer-controlled galvanostat (Shenzhen, China) at different rates at room temperature. The test rates were calculated on the basis of TiO_2 mass, and the detailed calculation and data (Figure S2) are given in the Supporting Information. Electrochemistry impedance spectroscopy (EIS) was conducted with a Princeton Applied Research instrument by applying an alternating current voltage of 10 mV in the frequency range from 0.01 Hz to 100 kHz.

RESULTS AND DISCUSSION

Figure 1a shows the typical XRD pattern of the $Ti_{15}Al_{85}$ source alloy, in which two sets of diffraction peaks can be indexed to the Al_3Ti alloy phase and pure Al, respectively. Because the atomic content of Al is fixed around 85 atom % in the refining process of the source alloy, the excess of Al is actually expected. This is beneficial to the following corrosion process. According to our previous work,[17,18] once the "active metal-Al" binary alloy (such as MnAl and CoAl alloys) was immersed in a NaOH solution, Al would be selectively etched by OH^-. With the Al atoms were etched, the remaining metal atoms become less coordinated, which would be exposed to OH^- ions and the oxygen-containing atmosphere. In such an alkaline environment, the freshly exposed metal atoms were so active that they would instantaneously combine with OH^- and undergo a natural oxidation by O_2, resulting in the formation of metal oxides. Therefore, etching of $Ti_{15}Al_{85}$ alloy foil was conducted in a 2 mol L^{-1} NaOH solution for 72 h at room temperature, and Figure 1b presents the XRD pattern of the collected sample upon dealloying the TiAl alloy. We found that no obvious diffraction peak emerged, indicating formation of an amorphous state. To improve our understanding of its structural composition, the sample was annealed at 600 °C for 4−8 h under the protection of N_2. Figure 1b also gives the XRD data of the sample after it has been annealed. By comparison, the amorphous sample presents a structure of anatase TiO_2 upon being annealed, suggesting that the freshly dealloyed sample should be amorphous TiO_2. Figure 1c further gives the composition analysis results of the fresh sample after it has been etched for 72 h based on EDS, and the elemental mapping of Ti and O is presented in Figure S1a−c of the Supporting Information. There is almost no residual Al atom detected on the basis of EDS analysis, which may be related to its overly low content and to the fact that EDS is not sensitive for the detection of the lower contents of some elements.

In addition, we used X-ray photoelectron spectroscopy (XPS) to characterize the resulting sample. As shown in Figure 1d, the two main peaks located at 458.2 and 464.0 eV can be assigned to Ti^{4+} $2p_{3/2}$ and Ti^{4+} $2p_{1/2}$ in TiO_2, respectively.[19] These results indicate that the product after the dealloying process is TiO_2. Moreover, we also detected the existence of Al. As shown in Figure S1d of the Supporting Information, the XPS analysis indicates that Al_2O_3 exists in the amorphous TiO_2 sample and the content of Al is ~0.7 atom %. Such a low level of Al_2O_3 has almost no effect on the performance of the TiO_2 sample in Li-ion batteries because of its insulating property.

Figure 2a reveals the SEM image of the as-made TiO_2 sample. It is found that its microstructure is uniform, and we

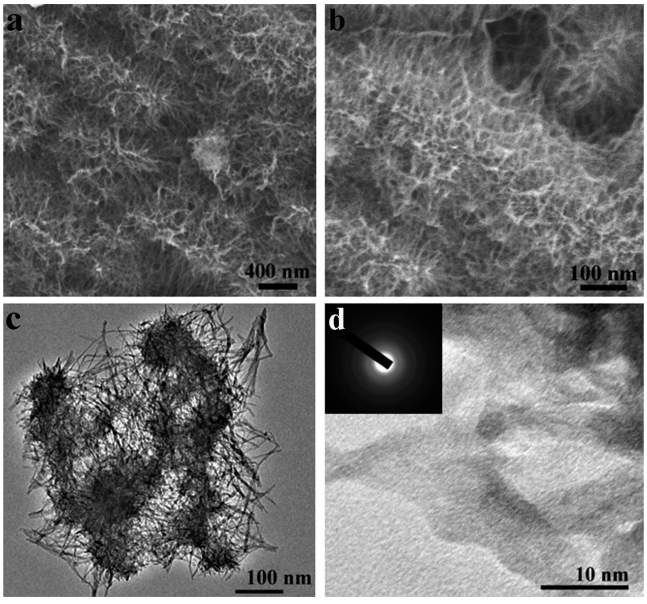

Figure 2. (a and b) SEM, (c) TEM, and (d) HRTEM SAED images of the freshly dealloyed TiAl alloy in a 2 M NaOH solution for 72 h.

can clearly observe that abundant nanowires interconnect with each other to build a three-dimensional (3D) network structure. Such a network structure runs through the whole sample. The cross-section SEM image (Figure 2b) indicates that the NaOH solution has penetrated the whole sample with uniform interconnected nanowires extending in three dimensions upon dealloying. In addition, TEM was employed to further characterize its microstructure. As shown in Figure 2c, it is clearly found that the network is well-structured by many ultrafine nanowires, which are measured to be ~5 nm in diameter. This is highly consistent with the SEM observation. A high-resolution TEM (HRTEM) image of the dealloyed sample provides the detailed structural information. As shown in Figure 2d, no clear lattice fringe was resolved, indicating the poor crystallinity of the freshly made TiO_2. In addition, the selected area electron diffraction (SAED) pattern (Figure 2d inset) also demonstrated the formation of amorphous TiO_2. These results are consistent with the observations obtained from the HRTEM image and the XRD study.

To improve our understanding of the formation and evolution of this 3D network structure during dealloying, we collected the product at different corrosion stages. As shown in Figure 3a, we find that the surface of the TiAl source alloy is smooth. When the alloy has been immersed in a NaOH solution for 0.5 h, the alloy surface becomes rough upon

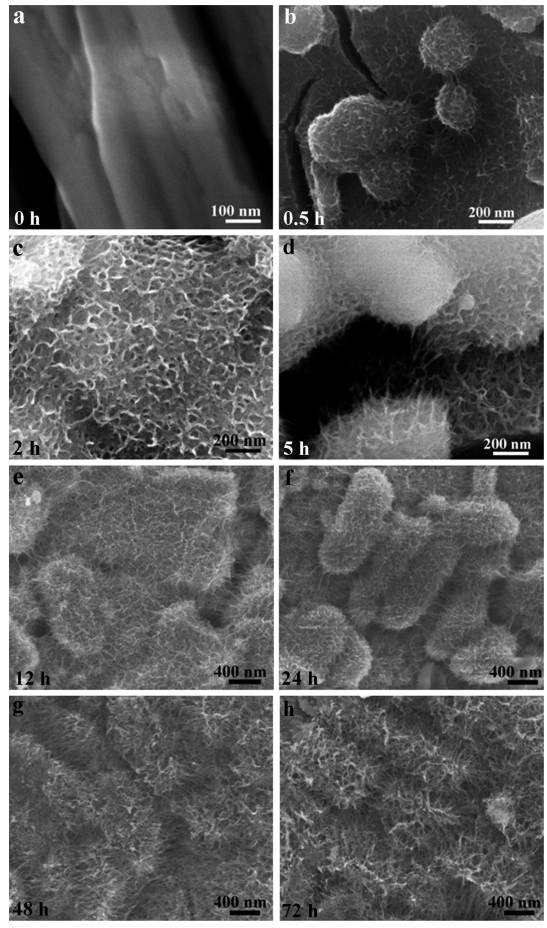

Figure 3. SEM images of the TiAl alloy immersed in a NaOH solution for different corrosion times.

corrosion (Figure 3b), and this corrosion phenomenon is more obvious with the extension of corrosion time (Figure 3c). Once the corrosion time reaches 5 h, some winding nanowires form on the alloy surface (Figure 3d), and many more nanowires are observed at a corrosion time of 12 h (Figure 3e). However, even when the etching time is extended to 24 h (Figure 3f), it is found that the inner structure under the interconnected nanowires is not completely etched with the solid substrate. Until the TiAl alloy is immersed for 48 h (Figure 3g), the etching process gradually permeates into the inner portion of the sample. When a sample is etched for 72 h (Figure 3h), almost all the Al atoms are dissolved with formation of the uniform 3D cross-linking TiO_2 nanowire network.

On the basis of the observation described above, structural evolution from the TiAl alloy to the TiO_2 network structure is illustrated by a scheme. As shown in Figure 4, the TiAl alloy is first immersed in a diluted NaOH solution at room temperature. Under such a mild etching condition, Al atoms are selectively dissolved in a NaOH solution. Meanwhile, Ti atoms are simultaneously oxidized by O_2 in an alkaline environment and self-assembled to form cross-linking nanowire-like TiO_2. This etching and oxidation process starts from the surface of the TiAl alloy and gradually extends to the inner portion of the alloy. Then, the final product has a bicontinuous network structure built by 3D cross-linking nanowires with the ongoing reaction.

Figure 5 presents the sustainable cycling performance of the amorphous TiO_2 as an anode material between 0.01 and 3 V

Figure 4. Schematic fabrication of the TiO_2 network structure.

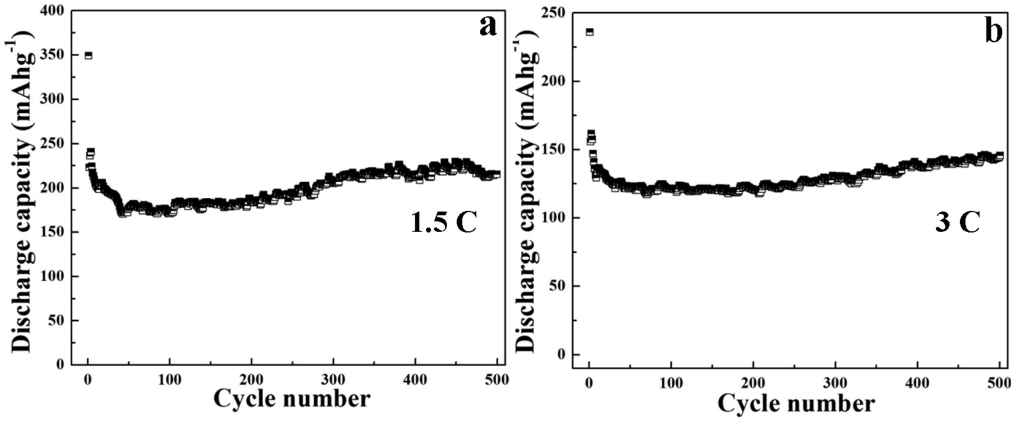

Figure 5. Cycling behavior of amorphous TiO_2 samples tested between 0.01 and 3 V (1.5 C = 500 mA g^{-1}, and 3 C = 1000 mA g^{-1}).

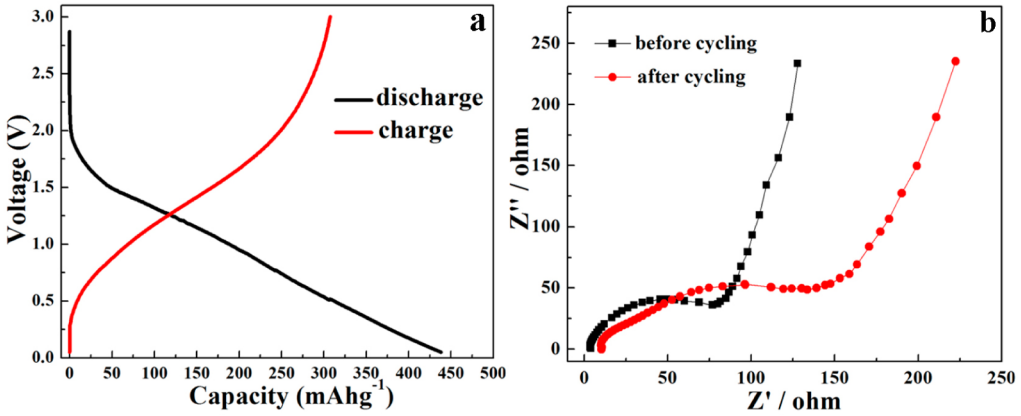

Figure 6. (a) Discharge–charge profiles of the amorphous TiO_2 sample at 1.5 C. (b) Impedance spectra of the amorphous TiO_2 network obtained before and after cycling.

and at high current densities of 1.5 and 3 C (1 C = 335 mA g^{-1}). (The capacities of TiO_2 are calculated by deducting the capacity of acetylene black from the measured capacities, and the detailed calculation method is described in the Supporting Information.) As shown in Figure 5a, its initial discharge capacity is 349.1 mA h g^{-1} at 1.5 C. Subsequently, a large irreversible capacity loss is observed in the following cycles. This is partly caused by the formation of solid electrolyte interface (SEI) films caused by the degradation of the electrolyte on the surface of TiO_2 and also partly related to the reaction of binding water in the TiO_2 with lithium to form Li_2O on the surface.[20−27] When for ∼50 cycles are conducted, the capacity drops to 170 mA h g^{-1}. However, it is interesting to find that the capacity exhibits an increasing trend from cycle 100 onward and remains at ∼215 mA h g^{-1} between cycles 300 and 500. The phenomenon of increasing capacity is attributed to the reversible growth of a polymeric gel-like film because of the kinetically activated electrolyte degradation. This is normally observed for transition metal oxides and has been explained well in refs 28−31.

A long cycling life at a high current density is an important property for an anode candidate electrode. Therefore, the test rate was fixed at 3 C (1000 mA g^{-1}). As shown in Figure 5b, the sample still delivers an initial capacity of 236 mA h g^{-1}. Similar to the performance at 1.5 C, the capacity exhibits fading in a few subsequent cycles. With additional cycles, it is striking to find that TiO_2 retains a reversible capacity of 120 mA h g^{-1}, which is stable even with a tendency to increase after ∼300 cycles and reaches 145 mA h g^{-1} at cycle 500. These results indicate the excellent cycling stability of the as-made amorphous TiO_2, which should be ascribed to its unique bicontinuous network structure providing a good mechanical support and electron conducting pathway.

Figure 6a shows the charge−discharge voltage profiles cycled at a current density of 1.5 C over the potential window of 0.01−3 V versus Li^+/Li (the capacity contains the contribution from TiO_2 and acetylene black). It is observed that no plateau is present in the charge−discharge curves of the amorphous TiO_2 electrode. This is in agreement with previously reported results for amorphous TiO_2.[9,32−35] In addition, electrochemical impedance spectroscopy (EIS) measurements were taken, and the typical Nyquist plots of the cells before and after charge−discharge cycling are shown in Figure 6b. For the cell before the cycling test, the Nyquist plot contains a depressed semicircle in

dx.doi.org/10.1021/am5010305 | ACS Appl. Mater. Interfaces 2014, 6, 10107−10112

the high-frequency region and a sloping line in the low-frequency region. The semicircle represents the charge transfer resistance (R_{ct}), and the inclined line reflects the Warburg impedance (Z_w), which is related to the solid-state diffusion of Li^+ in the electrode material. When the cell has been subjected to 500 cycles, the Nyquist plot comprises three parts. A semicircle appearing in the high-frequency region reflects the resistance due to the migration of Li^+ through the SEI film (Rsf); another semicircle in the medium-frequency region is related to R_{ct}, and a sloping line in the low-frequency range represents the Z_w.[36] Compared with the difference in the EIS results for the two cells, SEI films should form during the charge−discharge process.

Moreover, we also investigated the rate performance of amorphous TiO_2 to evaluate its power capability. As shown in Figure 7, the sample was first charge−discharge cycled at 0.6 C

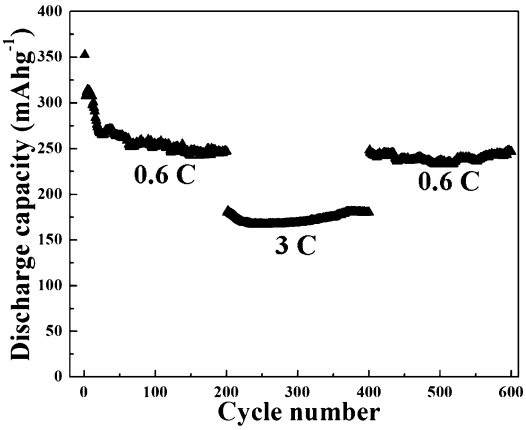

Figure 7. Rate performance of amorphous TiO_2.

(200 mA g^{-1}); we found that the capacity remained stable between cycles 100 and 200 and reached 245 mA h g^{-1} at cycle 200. Then the current density was increased to 3 C, while the capacity decreased to ∼175 mA g^{-1}. However, there is almost no capacity loss during the 200 tested cycles. Finally, the current density was decreased back to 0.6 C, and a stable capacity of ∼240 mA h g^{-1} could be recovered, which was close to the capacity at the previous rate of 0.6 C. These data demonstrate that the as-made amorphous TiO_2 sample has a good rate capability and great potential as a high-rate anode material for LIBs.

CONCLUSIONS

This work aimed to employ an effective and simple dealloying method to prepare TiO_2 anode material with high performance for LIBs. Amorphous TiO_2 network structure building with cross-linking nanowires were fabricated at room temperature with high throughput via a dealloying method. The charge−discharge cycling test manifested that the as-made TiO_2 delivered high and stable capacity even at a high rate of 1000 mA g^{-1} because of its unique continuous network structure, indicating the great application potential of the TiO_2 sample as anode materials with high activity and easy preparation.

ASSOCIATED CONTENT

Supporting Information

Elemental mapping, Al 2p XPS spectra of the amorphous TiO_2 sample, and the calculation process for deducting the contribution of acetylene black to the capacity. This material is available free of charge via the Internet at http://pubs.acs.org.

AUTHOR INFORMATION

Corresponding Author

*E-mail: chm_xucx@ujn.edu.cn.

Notes

The authors declare no competing financial interest.

ACKNOWLEDGMENTS

This work was supported by the National Science Foundation of China (21271085) and the Doctoral Foundation of the University of Jinan (XBS1314).

REFERENCES

(1) Whittingham, M. S. Lithium Batteries and Cathode Materials. *Chem. Rev.* **2004**, *104*, 4271−4302.
(2) Tarascon, J. M.; Armand, M. Issues and Challenges Facing Rechargeable Lithium Batteries. *Nature* **2001**, *414*, 359−367.
(3) Zhang, W. J. A Review of the Electrochemical Performance of Alloy Anodes for Lithium-Ion Batteries. *J. Power Sources* **2011**, *196*, 13−24.
(4) Zheng, H. H.; Qu, Q. T.; Zhang, L.; Liu, G.; Battalion, V. S. Hard Carbon: A Promising Lithium-Ion Battery Anode for High Temperature Applications with Ionic Electrolyte. *RSC Adv.* **2012**, *2*, 4904−4912.
(5) Wu, H. B.; Chen, J. S.; Hng, H. H.; Lou, X. W. Nanostructured Metal Oxide-Based Materials as Advanced Anodes for Lithium-Ion Batteries. *Nanoscale* **2012**, *4*, 2526−2542.
(6) Giannuzzi, R.; Manca, M.; De Marco, L.; Belviso, M. R.; Cannavale, A.; Sibillano, T.; Giannini, C.; Cozzoli, P. D.; Gigli, G. Ultrathin TiO_2(B) Nanorods with Superior Lithium-Ion Storage Performance. *ACS Appl. Mater. Interfaces* **2014**, *6*, 1933−1943.
(7) Han, B.; Kim, S. J.; Hwang, B. M.; Kim, S. B.; Park, K.-W. Single-Crystalline Rutile TiO_2 Nanowires for Improved Lithium Ion Intercalation Properties. *J. Power Sources* **2013**, *222*, 225−229.
(8) Hao, B.; Yan, Y.; Wang, X. B.; Chen, G. Synthesis of Anatase TiO_2 Nanosheets with Enhanced Pseudocapacitive Contribution for Fast Lithium Storage. *ACS Appl. Mater. Interfaces* **2013**, *5*, 6285−6291.
(9) Fang, H. T.; Liu, M.; Wang, D. W.; Sun, T.; Guan, D. S.; Li, F.; Zhou, J. G.; Sham, T. K.; Cheng, H. M. Comparison of the Rate Capability of Nanostructured Amorphous and Anatase TiO_2 for Lithium Insertion Using Anodic TiO_2 Nanotube Arrays. *Nanotechnology* **2009**, *20*, 225701.
(10) You, J. C.; Sheng, W. J.; Huang, K. K.; Hou, C. M.; Yue, H. J.; Hu, B.; Wang, M.; Wei, D. L.; Li, Q. W.; Zhao, L. P.; Dong, W. Y.; Zhao, Z. G.; Li, Y. J. Novel Cigarlike TiO_2 Nanofibers: Fabrication, Improved Mechanical, and Electrochemical Performances. *ACS Appl. Mater. Interfaces* **2013**, *5*, 2278−2282.
(11) Lee, S.; Ha, J.; Choi, J.; Song, T.; Lee, J. W.; Paik, U. 3D Cross-Linked Nanoweb Architecture of Binder-free TiO_2 Electrodes for Lithium Ion Batteries. *ACS Appl. Mater. Interfaces* **2013**, *5*, 11525−11529.
(12) Tsuchiya, H.; Macak, J. M.; Taveira, L.; Balaur, E.; Ghicov, A.; Sirotna, K.; Schmuki, P. Self-Organized TiO_2 Nanotubes Prepared in Ammonium Fluoride Containing Acetic Acid Electrolytes. *Electrochem. Commun.* **2005**, *7*, 576−580.
(13) Lee, K. H.; Song, S. W. One-Step Hydrothermal Synthesis of Mesoporous Anatase TiO_2 Microsphere and Interfacial Control for Enhanced Lithium Storage Performance. *ACS Appl. Mater. Interfaces* **2011**, *3*, 3697−3703.
(14) Liu, S. M.; Gan, L. M.; Lu, L. H.; Zhang, W. D.; Zheng, H. C. Synthesis of Single-Crystalline TiO_2 Nanotubes. *Chem. Mater.* **2002**, *14*, 1391−1397.
(15) Wang, H. E.; Lu, Z. G.; Xi, L. J.; Ma, R. G.; Wang, C. D.; Zapien, J. A.; Bello, I. Facile and Rapid Synthesis of Highly Porous Wirelike

TiO_2 as Anodes for Lithium-Ion Batteries. *ACS Appl. Mater. Interfaces* **2012**, *4*, 1608−1615.
(16) Chang, Y. C.; Lee, C. Y.; Chiu, H. T. Porous Inorganic Materials from Living Porogens: Channel-like TiO_2 from Yeast-Assisted Sol-Gel Process. *ACS Appl. Mater. Interfaces* **2014**, *6*, 31−35.
(17) Hao, Q.; Li, M. H.; Jia, S. Z.; Zhao, X. Y.; Xu, C. X. Controllable Preparation of Co_3O_4 Nanosheets and Their Electrochemical Performance for Li-Ion Batteries. *RSC Adv.* **2013**, *3*, 7850−7854.
(18) Hao, Q.; Wang, J. P.; Xu, C. X. Facile Preparation of Mn_3O_4 Octahedra and Their Long-Term Cycle Life as An Anode Material for Li-Ion Batteries. *J. Mater. Chem. A* **2014**, *2*, 87−93.
(19) Zhao, J. Y.; Yao, J. X.; Zhang, Y. Z.; Guli, M. N.; Xiao, L. Effect of Thermal Treatment on TiO_2 Nanorod Electrodes Prepared by the Solvothermal Method for Dye-sensitized Solar Cells: Surface Reconfiguration and Improved Electron Transport. *J. Power Sources* **2014**, *255*, 16−23.
(20) Xiao, Y.; Hu, C. W.; Cao, M. H. Compositing Amorphous TiO_2 with N-Doped Carbon as High-Rate Anode Materials for Lithium-Ion Batteries. *Chem.—Asian J.* **2014**, *9*, 351−356.
(21) Wang, W. S.; Sa, Q.; Chen, J. H.; Wang, Y.; Jung, H. J.; Yin, Y. D. Porous TiO_2/C Nanocomposite Shells As a High-Performance Anode Material for Lithium-Ion Batteries. *ACS Appl. Mater. Interfaces* **2013**, *5*, 6478−6483.
(22) Han, H.; Song, T.; Lee, E. K.; Devadoss, A.; Jeon, Y.; Ha, J.; Chung, Y. C.; Choi, Y. M.; Jung, Y. G.; Paik, U. Dominant Factors Governing the Rate Capability of a TiO_2 Nanotube Anode for High Power Lithium Ion Batteries. *ACS Nano* **2012**, *6*, 8308−8315.
(23) Wang, Y. F.; Wu, M. Y.; Zhang, W. F. Preparation and Electrochemical Characterization of TiO_2 Nanowires as an Electrode Material for Lithium-Ion Batteries. *Electrochim. Acta* **2008**, *53*, 7863−7868.
(24) Liu, L. C.; Fan, Q.; Sun, C. Z.; Gu, X. R.; Li, H.; Gao, F.; Chen, Y. F.; Dong, L. Synthesis of Sandwich-like TiO_2@C Composite Hollow Spheres with High Rate Capability and Stability for Lithium-ion Batteries. *J. Power Sources* **2013**, *221*, 141−148.
(25) Song, B.; Liu, S.; Jian, J.; Lei, M.; Wang, X.; Li, H.; Yu, J.; Chen, X. Electrochemical Properties of TiO_2 Hollow Microspheres from a Template-Free and Green Wet-Chemical Route. *J. Power Sources* **2008**, *180*, 869−874.
(26) Tang, Y. P.; Wu, D. Q.; Chen, S.; Zhang, F.; Jia, J. P.; Feng, X. L. Highly Reversible and Ultra-Fast Lithium Storage in Mesoporous Graphene-Based TiO_2/SnO_2 Hybrid Nanosheets. *Energy Environ. Sci.* **2013**, *6*, 2447−2451.
(27) Singh, D. P.; George, A.; Kumar, R. V.; Elshof, J. E.; Wagemaker, M. Nanostructured TiO_2 Anatase Micropatterned Three-Dimensional Electrodes for High-Performance Li-Ion Batteries. *J. Phys. Chem. C* **2013**, *117*, 19809−19815.
(28) Laruelle, S.; Grugeon, S.; Poizot, P.; Dolle, M.; Dupont, L.; Tarascon, J. M. On the Origin of the Extra Electrochemical Capacity Displayed by MO/Li Cells at Low Potential. *J. Electrochem. Soc.* **2002**, *149*, A627−A634.
(29) Grugeon, S.; Laruelle, S.; Dupont, L.; Tarascon, J. M. An Update on the Reactivity of Nanoparticles Co-Based Compounds Towards Li. *Solid State Sci.* **2003**, *5*, 895−904.
(30) Zhou, G. M.; Wang, D. W.; Li, F.; Zhang, L. L.; Li, N.; Wu, Z. S.; Wen, L.; Lu, G. Q.; Cheng, H. M. Graphene-Wrapped Fe_3O_4 Anode Material with Improved Reversible Capacity and Cyclic Stability for Lithium Ion Batteries. *Chem. Mater.* **2010**, *22*, 5306−5313.
(31) Do, J. S.; Weng, C. H. Preparation and Characterization of CoO Used as Anodic Material of Lithium Battery. *J. Power Sources* **2005**, *146*, 482−486.
(32) Furukawa, H.; Hibino, M.; Honma, I. Electrochemical Properties of Nanostructured Amorphous, Sol-Gel-Synthesized TiO_2/Acetylene Black Composite Electrodes. *J. Electrochem. Soc.* **2004**, *151*, A527−A531.
(33) Hibino, M.; Abe, K.; Mochizuki, M.; Miyayama, M. Amorphous Titanium Oxide Electrode for High-Rate Discharge and Charge. *J. Power Sources* **2004**, *126*, 139−143.
(34) Borghols, W.; Lutzenkirchen-Hecht, D.; Haake, U.; Chan, W.; Lafont, U.; Kelder, E. M.; van Eck, E.; Kentgens, A.; Mulder, F. M.; Wagemaker, M. Lithium Storage in Amorphous TiO_2 Nanoparticles. *J. Electrochem. Soc.* **2010**, *157*, A582−A588.
(35) Ban, C. M.; Xie, M.; Sun, X.; Travis, J. J.; Wang, G. K.; Sun, H. T.; Dillon, A. C.; Lian, J.; George, S. M. Atomic Layer Deposition of Amorphous TiO_2 on Graphene as an Anode for Li-Ion Batteries. *Nanotechnology* **2013**, *24*, 424002.
(36) Shaju, K. M.; Jiao, F.; Débarta, A.; Bruce, P. G. Mesoporous and Nanowire Co_3O_4 as Negative Electrodes for Rechargeable Lithium Batteries. *Phys. Chem. Chem. Phys.* **2007**, *9*, 1837−1842.